doi.org/10.1002/cbdv.202201206

RESEARCH ARTICLE

CHEMISTRY & BIODIVERSITY

New Combretastatin Analogs as Anticancer Agents: Design, Synthesis, Microtubules Polymerization Inhibition, and Molecular Docking Studies

Shaker A. Abdul Hussein,[a] Ammar A. Razzak Mahmood,[b] Lubna H. Tahtamouni,*[c, d] Asim A. Balakit,[a] Yahya S. Yaseen,[e] and Rehab A. Al-Hasani[f]

[a] Department of Pharmaceutical Chemistry, College of Pharmacy, University of Babylon, 51001 Babylon, Iraq
[b] Department of Pharmaceutical Chemistry, College of Pharmacy, University of Baghdad, 10001 Baghdad, Iraq
[c] Department of Biology and Biotechnology, Faculty of Science, The Hashemite University, 13133 Zarqa, Jordan
[d] Department of Biochemistry and Molecular Biology, College of Natural Sciences, Colorado State University, Fort Collins, 80523 Colorado, USA, e-mail: lubna.tahtamouni@colostate.edu
[e] Department of Pharmaceutical Chemistry, College of Pharmacy, University of Tikrit, 34001 Tikrit, Iraq
[f] Department of Chemistry, College of Science, Al-Mustansiriyah University, 10052 Baghdad, Iraq

A new series of 4-(4-methoxyphenyl)-5-(3,4,5-trimethoxyphenyl)-4*H*-1,2,4-triazole-3-thiol derivatives were synthesized as analogs for the anticancer drug **combretastatin A-4** (**CA-4**) and characterized using FT-IR, ^{1}H-NMR, ^{13}CNMR, and HR-MS techniques. The new **CA-4** analogs were designed to meet the structural requirements of the highest expected anticancer activity of **CA-4** analogs by maintaining ring **A** 3,4,5-trimethoxyphenyl moiety, and at the same time varying the substituents effect of the triazole moiety (ring **B**). *In silico* analysis indicated that compound **3** has higher total energy and dipole moment than **colchicine** and the other analogs, and it has excellent distribution of electron density and is more stable, resulting in an increased binding affinity during tubulin inhibition. Additionally, compound **3** was found to interact with three apoptotic markers, namely p53, Bcl-2, and caspase 3. Compound **3** showed strong similarity to **colchicine**, and it has excellent pharmacokinetics properties and a good dynamic profile. The *in vitro* anti-proliferation studies showed that compound **3** is the most cytotoxic **CA-4** analog against cancer cells (IC_{50} of 6.35 μM against Hep G2 hepatocarcinoma cells), and based on its selectivity index (4.7), compound **3** is a cancer cytotoxic-selective agent. As expected and similar to **colchicine**, compound **3**-treated Hep G2 hepatocarcinoma cells were arrested at the G2/M phase resulting in induction of apoptosis. Compound **3** tubulin polymerization IC_{50} (9.50 μM) and effect on V_{max} of tubulin polymerization was comparable to that of **colchicine** (5.49 μM). Taken together, the findings of the current study suggest that compound **3**, through its binding to the colchicine-binding site at β-tubulin, is a promising microtubule-disrupting agent with excellent potential to be used as cancer therapeutic agent.

Keywords: combretastatin **A-4**, MTT assay, cell cycle, apoptosis, tubulin polymerization.

Introduction

Cancer is a life threatening condition characterized by uncontrolled cell growth and abnormal cell division.[1] Targeted antineoplastic compounds have grown in popularity as effective cancer therapeutic options, with pharmaceutical companies focusing on targeted medications against different and distinct cancer types.[2] Tubulin assembly inhibitors are one of the most well-known and effective types of such targeted chemotherapeutic medicines.[3]

Microtubules (MTs) are synthesized by the interaction of α- and β-tubulin heterodimers in a head-

Supporting information for this article is available on the WWW under https://doi.org/10.1002/cbdv.202201206

and-tail fashion to form hollow cylindrical tubes with a diameter of 25 nm.[4–7] Several key cellular functions including motility, cell division, secretion, communication, and shape maintenance are carried out by MTs.[8–10] These various roles have made the microtubule system an attractive target for cancer chemotherapy.[11,12] Disruption of MTs dynamics causes cell cycle arrest at the G2/M phase and induces apoptosis.[13,14] **Taxol**, **vincristine**, and **colchicine**, all of which are derived from natural products, are only a few of the microtubule-interfering agents (MIAs) that have been discovered. These MIAs bind to β-tubulin at specific sites known as taxol-, Vinca-, and colchicine-binding sites, respectively, in which they can either stimulate or inhibit tubulin polymerization.[15] Due to their beneficial effects on ATP-binding cassette (ABC)-transporter-mediated drug resistance, colchicine-binding site inhibitors are receiving a lot of interest right now.[16,17]

Several studies have reported that the most effective antimitotic agent of this class against a variety of tumor cells is **combretastatin A-4** (**CA-4**).[18] **CA-4** was isolated from the South African willow species *Combretum caffrum's* bark in 1989.[19] **CA-4** binds to colchicine-binding site on β-tubulin and inhibits microtubule polymerization,[20] additionally, it obstructs blood flow to solid tumors and disrupts the vasculature of tumor cells causing cell death (apoptosis).[21–23] Due to its structural simplicity, **CA-4** has been investigated as a leading pharmacophore to understand tubulin activities and characteristics.[24] Studies using **CA-4** Structure-Activity Relationship (SAR) have identified three crucial structural elements essential for its anti-tubulin activity. These include (i) the 3,4,5-trimethoxy moiety on ring A; (ii) the *cis*-configuration bridge (B) of both aromatic rings (the *trans*-orientation is inactive); and (iii) the presence of a small substituent on ring C, such as a methoxy group (*Figure 1A*). The aromatic rings in **CA-4** can adopt the best binding orientation for interactions with colchicine-binding site on β-tubulin thanks to the *cis*-alkene structure. Unfortunately, **CA-4** tends to isomerize from its active *cis*-configuration to its inactive *trans*-configuration during storage and during *in vivo*

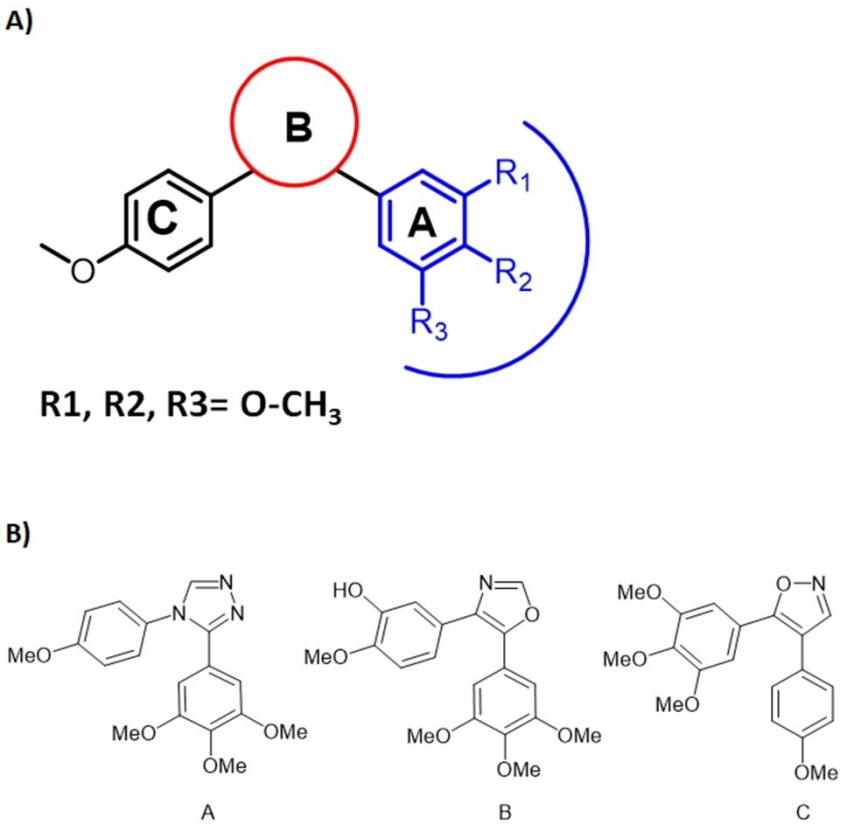

Figure 1. Structures of **combretastatin A-4** (**CA-4**) and **CA-4** analogs. A) Crucial structural elements of **combretastatin A-4** (**CA-4**) required for its anti-tubulin activity. B) Modified **combretastatin A-4** analogs by replacing the *cis* double bond by heterocyclic ring: triazole in compound **a**; oxazole in compound **b**; and isoxazole in compound **c**.

metabolism.[25–27] Many structural changes to **CA-4** have been made to get around this by replacing the *cis* double bond with monocyclic heterocycles, such as triazole, oxazole, and isoxazole to produce **CA-4** analogs shown in *Figure 1B*.[26–31] Previous studies have shown that these **CA-4** analogs exhibit strong anti-proliferation activities against a variety of cancer cell lines.[32]

In the current study, we report the design and synthesis of new 1,2,4-triazole **CA-4** analogs with aliphatic, alicyclic, aromatic, and substituted phenyl isothiocyanate groups attached to the thioacetohydrazide group (ring B). The new compounds were designed to meet the structural requirements of the highest expected anticancer activity of **CA-4** analogs by maintaining the 3,4,5-trimethoxyphenyl moiety present in ring **A** of **CA-4**, and at the same time varying the substituents effect of the triazole moiety. The mode of action of the newly synthesized analogs and their anti-proliferative effects against several cancer cell lines were investigated *in silico* and *in vitro*. The results presented should improve our understanding of the mechanisms behind the compounds' capacity to disrupt microtubules polymerization and provide guidance for future investigations into potent anticancer drugs.

Result and Discussion

Chemistry

The intermediates of the newly synthesized **CA-4** analogs' 1,2,4-triazole scaffold was obtained in three successive phases using commercially available 3,4,5-trimethoxy benzoic acid. The overall process for synthesizing the desired 1,2,4 triazole **CA-4** analogs is depicted in *Scheme 1*. Compounds **S1** and **S2** were synthesized and characterized based on previous research.[33] Compound **S2** (ester) was treated with hydrazine hydrate to produce the hydrazide derivative (compound **1**).[34] Compound **1** was treated with ethyl acetoacetate or tetrahydro-

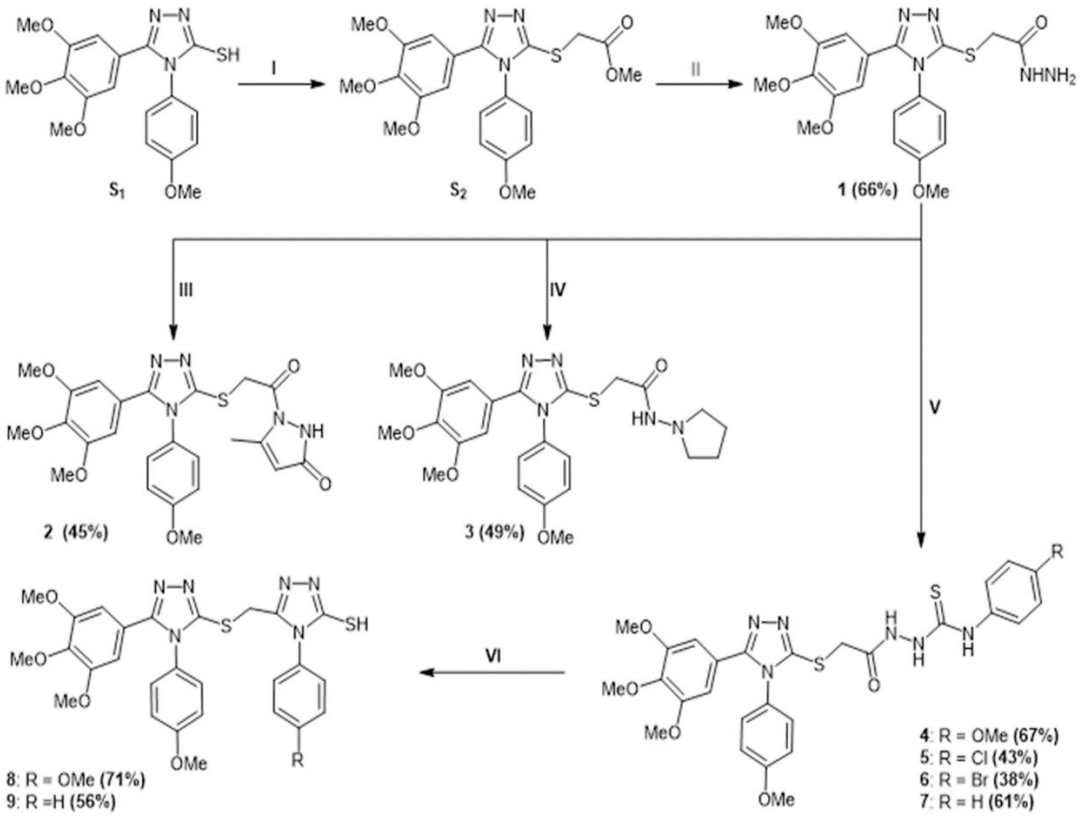

Scheme 1. The synthetic pathway for the preparation of target compounds S2 and 1–9.

furan to yield compounds **2** and **3**, respectively.[34] Additionally, compound **1** was treated with different para-substituted phenyl isothiocyanates to produce compounds **4**–**7**.[35] Compounds **8** and **9** were synthesized by heating compounds **4** and **7** with 2 N NaOH, respectively (*Scheme 1*).[36]

The IR spectrum of compound **1** revealed bands at 3307 and 3141 cm^{-1}, attributed to *asymmetric* and *symmetric* NH_2 stretching, respectively, at 3224 cm^{-1} a stretching band related to NH of the hydrazide moiety, (**NH**-NH_2), and a characteristic band at 1672 cm^{-1}, attributed to the (C = O)) group. Compound **2**'s IR spectrum revealed a new (C=O) band at 1736 cm^{-1}.. The IR spectrum of compound **3** indicated a secondary (N–H) band at 3204 cm^{-1}, and another band due to (C=O) amide at 1672 cm^{-1}. The IR spectra of compounds (**4**–**7**) revealed characteristic absorption bands for (Ar–N–H) amine at 3300–3288 cm^{-1}, the (NH–NH) secondary amine appeared at 3218–3151 cm^{-1}. Compounds **8** and **9**'s IR spectra revealed bands at 3011–3003 cm^{-1} for (Ar–CH), 2964 and 2837 cm^{-1} for aliphatic (C–H) for compound **8**, and 2934 and 2837 cm^{-1} for compound **9**. A distinct band at 1607 cm^{-1} due to (C=N) was observed, and another band at 1247 cm^{-1} due to (Ar C–O). Compounds **8** and **9**'s IR spectra revealed the disappearance of all (C=O) and (NH) bands (*Supplementary Figure 1*).

The interpretation of the ^{1}H-NMR spectrum (*Supplementary Figure 2*) for compound **1** (hydrazide) revealed a *singlet* peak at $\delta = 9.34$ ppm due to the (NH) group, and a *singlet* peak at $\delta = 4.30$ ppm owing to the hydrazide-(NH_2) group. Compound **2** showed distinct signals at $\delta = 11.36$ ppm attributed to the cyclic (NH) group, $\delta = 4.47$ ppm as a *singlet* assigned for (C=C–H), and $\delta = 2.15$ ppm attributed to the (CH_3) group. Compound **3**'s spectrum confirmed a signal, as a *singlet* at $\delta = 10.31$ ppm, due to the (NH) group, and all the aromatic protons were visible in their respective region. The spectra of compounds **4**–**7** revealed considerable signals at $\delta = 10.48$–10.40 ppm due to aromatic amines. The aromatic protons displayed properly at their distinct region. Furthermore, the spectra of compounds **8** and **9** displayed signals attributed to (NH-thione) at $\delta = 13.80$ and 13.87 ppm, respectively.

The ^{13}CNMR spectrum of compound **1** (*Supplementary Figure 3*) revealed a signal at $\delta = 166.54$ ppm due to (C=O) group, and another distinct signal at $\delta = 34.62$ ppm attributed to the (CH_2) group. Compound **2**'s ^{13}CNMR spectrum demonstrated a signal at $\delta = 166.45$ ppm owing to the (C=O) group, and a signal at $\delta = 100.18$ ppm related to the (CH=C) of the 5-methyl-1,2-dihydro-3*H*-pyrazol-3-one ring. Compound **3**'s spectrum confirmed a signal at $\delta = 167.84$ ppm attributed to the (C=O) amide, at $\delta = 20.99$ ppm due to the CH_2 group. The ^{13}CNMR spectra of compounds **4**–**7** indicated a signal at $\delta = 181.26$–180.65 ppm attributed to the (C=S) group, and a signal at $\delta = 160.75$–166.87 ppm assigned for the (C=O) group. Compounds **8** and **9**'s ^{13}CNMR spectra demonstrated signals at $\delta = 168.94$ and 168.72 ppm due to (C=S⇌C–S), respectively, and signals at $\delta = 27.83$ and 27.91 ppm due to (CH_2) group.

All compounds' mass spectra (*Supplementary Figure 4*) are distinguished by the presence of distinct molecular ion peaks at the predicted *m/z* values.

Molecular Docking

In silico *Binding Modes*

The binding modes and interaction energy (ΔG) of **colchicine** and the newly synthesized **CA-4** analogs to human tubulin are shown in *Figures 2* and *3*, and *Supplementary Table 1*. The binding mode of **colchicine** to human tubulin exhibited an interaction energy of −13.50 kcal/mol. The tetramethoxy-9-oxo-5,6,7,9-tetrahydrobenzo[a]heptalen-7-yl l moiety formed eleven *pi*-sulfur, and *pi*-alkyl interactions with Lys352, Ala316, Leu248, Cys241, Ala250, Leu255, Ala180, and Met259, and two H-bonds with Cys241 and Val181 (2.23 and 2.04 Å). Additionally, the acetamide group interacted with Asn101 by one H- bond (2.64 Å) (*Figure 2A*).

The binding mode of compound **1** exhibited an interaction energy of −12.97 kcal/mol against human tubulin. The 4-methoxyphenyl moiety created four *pi*-alkyl interactions with Ala180, Val181, Lys325, and Ala316. Additionally, the 3,4,5-trimethoxyphenyl moiety interacted with Cys241 by one H-bond (2.28 Å), and five *pi*-alkyl interactions with Leu255, Ala250, Cys241, Leu248, and Ala316, while the 4*H*-1,2,4-triazol-3-yl)thio) acetohydrazide moiety formed four *pi*-alkyl, *pi-pi*, and *pi*-sulfur interactions with Val180, Asn101, Lys254, and Ala250. Moreover, it interacted with Ser178 by one H-bond with (1.95 Å) (*Figure 2B*).

The binding mode of compound **2** showed an interaction energy of −13.02 kcal/mol against human tubulin. The 4-methoxyphenyl moiety produced two *pi*-alkyl interactions with Lys325 and Leu248, additionally, the 3,4,5-trimethoxyphenyl moiety interacted with Cys241 by one H-bond (2.76 Å), and four *pi*-alkyl

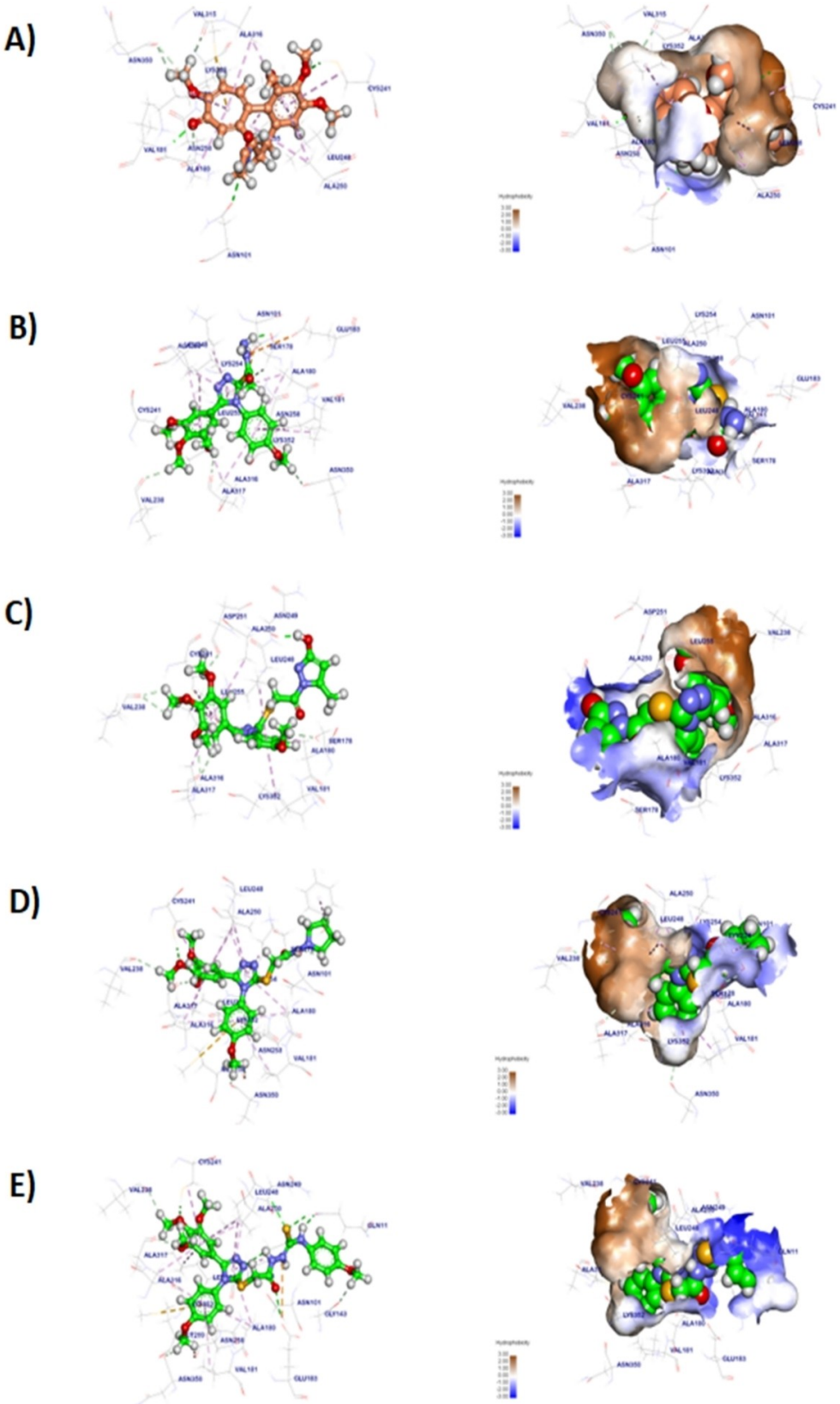

Figure 2. Docking of **colchicine** and **CA-4** derivatives **1**–**4** in human tubulin active pocket. A) **Colchicine**, B) Compound **1**, C) Compound **2**, D) Compound **3**, E) Compound **4**. Hydrogen bonds are shown in green lines, and the *pi* interactions are represented in purple lines.

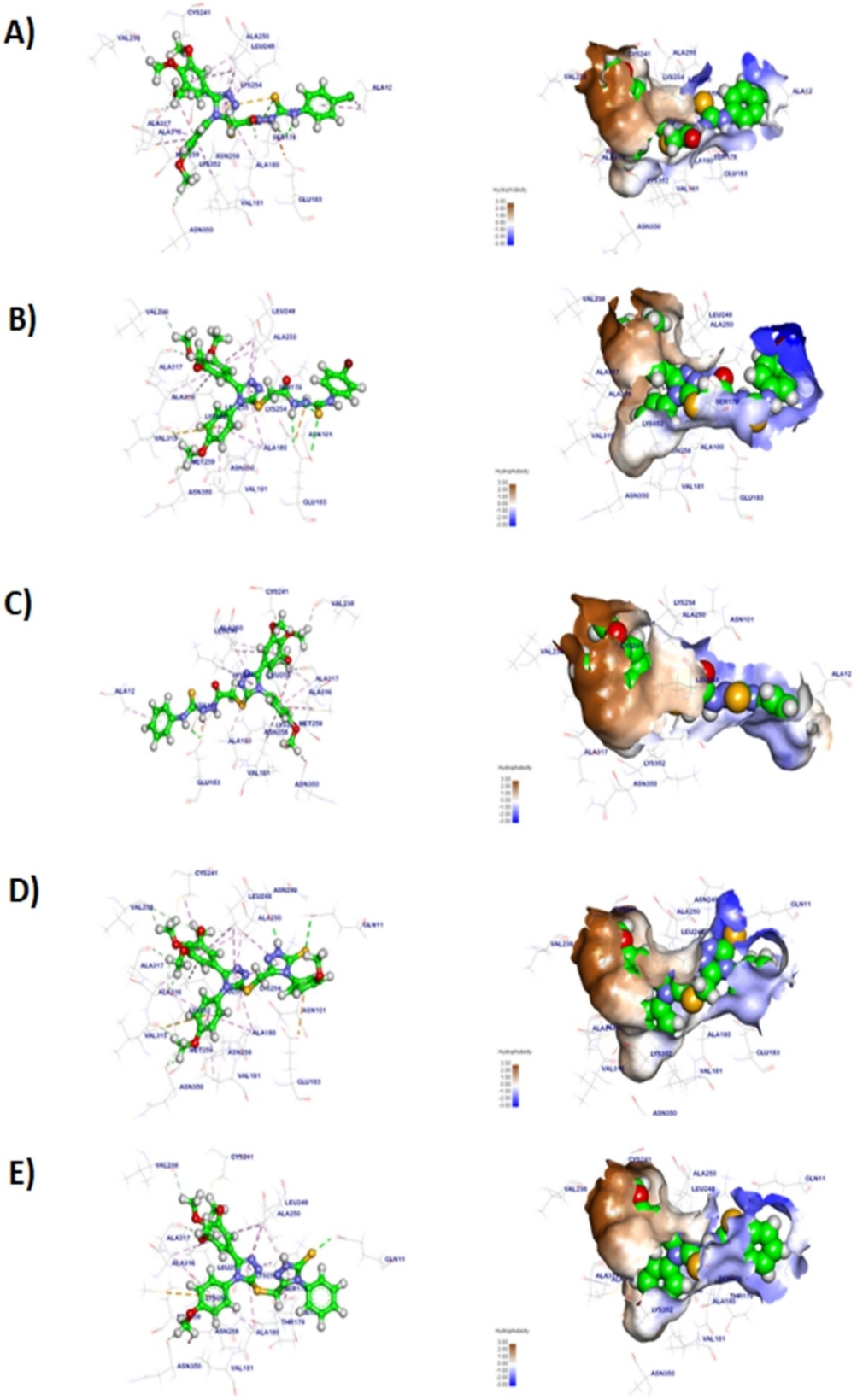

Figure 3. Docking of **CA-4** derivatives **5**–**9** in human tubulin active pocket. A) Compound **5**, B) Compound **6**, C) Compound **7**, D) Compound **8**, E) Compound 9. Hydrogen bonds are shown in green lines, and the *pi* interactions are represented in purple lines.

interactions with Leu255, Ala250, Cys241, and Ala316, while the 4*H*-1,2,4-triazol-3-yl)thio)acetyl)-5-methyl-1,2-dihydro-3*H*-pyrazol-3-one moiety formed two *pi*-alkyl interactions with Ala180 and Leu255. Moreover, it interacted with Asn249 by one H-bond (1.99 Å) (*Figure 2C*).

The binding mode of the hit compound **3** displayed an interaction energy of −14.16 kcal/mol against human tubulin. The 4-methoxyphenyl moiety created five *pi*-alkyl and *pi*-sulfur interactions with Ala180, Val181, Lys352, Met259, and Ala316. Additionally, the 3,4,5-trimethoxyphenyl moiety interacted with Cys241 by one H-bond (2.46 Å), and five *pi*-alkyl interactions with Leu255, Ala250, Cys241, Leu248, and Ala316, while the 4*H*-1,2,4-triazol-3-yl)thio)-*N*-(pyrrolidin-1-yl)acetamide moiety generated five *pi*-alkyl interactions with Leu248, Tyr224, Lys254, and Ala250, and it interacted with Ser178 by one H-bond (2.07 Å) (*Figure 2D*).

The binding mode of the candidate compound **4** exhibited an energy binding of −15.42 kcal/mol against human tubulin. The 4-methoxyphenyl moiety produced five *pi*-alkyl and *pi*-sulfur interactions with Ala180, Val181, Lys352, Met259, and Ala316, additionally, the 3,4,5-trimethoxyphenyl moiety interacted with Cys241 by one H-bond (2.43 Å), and five *pi*-alkyl interactions with Leu255, Ala250, Cys241, Leu248, and Ala316, while the *N*-(4-methoxyphenyl)-4*H*-1,2,4-triazol-3-yl)thio)acetyl) hydrazine-1-carbothioamide moiety formed four *pi*-alkyl interactions with Leu248, Lys254, and Ala250. Moreover, it interacted with Asn248 and Gln11 by three H-bonds (2.86, 2.74 and 2.18 Å) (*Figure 2E*).

The mode of binding of compound **5** exhibited an interaction energy of −15.14 kcal/mol against human tubulin. The 4-methoxyphenyl moiety generated four *pi*-alkyl interactions with Leu255, Lys352, Met259, and Ala316. Additionally, the 3,4,5-trimethoxyphenyl moiety interacted with Cys241 by one H-bond (2.51 Å), and by five *pi*-alkyl interactions with Leu255, Ala250, Cys241, Leu248, and Ala316. The *N*-(4-chlorophenyl)-4*H*-1,2,4-triazol-3-yl)thio)acetyl)hydrazine-1-carbothioamide moiety formed four *pi*-alkyl interactions with Ala12, Leu248, Lys254, Ala180, and Ala250, and it interacted with Asn101 and Ser178 by three H-bonds (2.22, 2.85 and 3.34 Å) (*Figure 3A*).

The binding mode of compound **6** revealed an interaction energy of −15.70 kcal/mol against human tubulin. The 4-methoxyphenyl moiety generated four *pi*-alkyl interactions with Val181, Ala180, Met259, and Ala316. Additionally, the 3,4,5-trimethoxyphenyl moiety interacted *via* five *pi*-alkyl interactions with Leu255, Ala250, Leu248, and Ala316, while the *N*-(4-bromophenyl)-4*H*-1,2,4-triazol-3-yl)thio)acetyl) hydrazine-1-carbothioamide moiety formed four *pi*-alkyl interactions with Ala180, Leu248, Lys254, and Ala250, and it interacted with Glu183 (*Figure 3B*).

The binding mode of the hit compound **7** exhibited binding energy of −15.86 kcal/mol against human tubulin. The 4-methoxyphenyl moiety created four *pi*-alkyl interactions with Leu255, Lys352, Met259, and Ala316. Additionally, the 3,4,5-trimethoxyphenyl moiety interacted with Cys241 by one H-bond (2.45 Å), and five *pi*-alkyl interactions with Leu255, Ala250, Cys241, Leu248, and Ala316, while the 4*H*-1,2,4-triazol-3-yl)thio)acetyl)-*N*-phenylhydrazine-1-carbothioamide moiety produced four *pi*-alkyl interactions with Ala12, Lys254, Ala180, and Ala250. Moreover, it interacted with Glu183 by H- bond (2.34 Å) (*Figure 3C*).

The binding mode of compound **8** showed an interaction energy of −14.41 kcal/mol against human tubulin. The 4-methoxyphenyl moiety produced six *pi*-alkyl interactions with Val181, Val180, Lys352, Met259, and Ala316. Additionally, the 3,4,5-trimethoxyphenyl moiety interacted *via* five *pi*-alkyl interactions with Leu255, Ala250, Cys241, Leu248, and Ala316, while the tetramethoxy-9-oxo-5,6,7,9-tetrahydrobenzo[a]-heptalen-7-yl l moiety formed eleven *pi*-sulfur, and *pi*-alkyl interactions with Lys352, Ala316, Leu248, Cys241, Ala250, Leu255, Ala180, and Met259, and two H-bonds with Cys241 and Val181 (2.23 and 2.04 Å).

Compound's **9** binding mode showed an interaction energy of −14.92 kcal/mol against human tubulin. The 4-methoxyphenyl moiety produced four *pi*-sulfur and *pi*-alkyl interactions with Ala180, Lys352, Met259, and Ala316. Additionally, the 3,4,5-trimethoxyphenyl moiety interacted by five *pi*-alkyl interactions with Leu255, Ala250, Leu248, and Ala316, while the 4*H*-1,2,4-triazol-3-yl)thio)methyl)-4-phenyl-4*H*-1,2,4-triazole-3-thiol moiety formed six *pi*-alkyl interactions with Ser178, Lys254, Leu248, Ala180, and with Gln11 by H-bond (2.48 Å) (*Figure 3E*).

The binding modes of **colchicine** and compound **3**, the most potent among the newly synthesized **CA-4** analogs (see below) against p53, caspase 3, and Bcl-2, are summarized in *Supplementary Figure 5* and *Supplementary Table 2*. The binding mode of **colchicine** exhibited a binding energy of −7.58 kcal/mol against p53 protein. **Colchicine** interacted with Pro13 and Gln72 by two Hbonds with a distance of 2.37 and 1.66 Å, and it formed sixteen *pi*-alkyl interactions with Val93, Ile61, His96, Ile99, Tyr100, Leu54, Phw91, Leu14, Phe86, Leu57, and Met62 (*Supplementary Figure 5A*). The best pose of compound **3** exhibited a binding

energy of −7.56 kcal/mol against p53. It interacted with Gln72 by a H-bond with a distance of 2.23 Å, additionally, compound **3** interacted with Tyr67, Ile61, Val93, and Leu54 by *pi*-alkyl interaction (*Supplementary Figure 5B*).

The binding mode of **colchicine** against caspase 3 exhibited a binding energy of −6.13 kcal/mol. It interacted with Leu168, Thr166, and Thr166 by three H-bonds with a distance of 2.03, 2.20 and 1.93 Å, moreover, it formed four *pi*-alkyl and *pi*-sigma interactions with Phe256, Leu168, and Phe256 (*Supplementary Figure 5C*). The best pose of compound **3** exhibited a binding energy of −7.70 kcal/mol against Caspase 3. It interacted with Thr166 by one H-bond with a distance of 2.08 Å, additionally, it interacted with Leu168 by two *Pi*-Alkyl interactions (*Supplementary Figure 5D*).

The binding mode of **colchicine** exhibited a binding energy of −7.60 kcal/mol against the anti-apoptotic protein Bcl-2. **Colchicine** interacted with Ala149 by a H-bond with a distance of 1.65 Å, and it formed twelve *pi*-alkyl, *pi*-sigma, *pi-pi*, *pi*-anion, and *pi*-cation interactions with Val133, Leu137, Met115, Asp111, Phe112, Tyr108, Phe104, and Ala149 (*Supplementary Figure 5E*). The best pose of compound **3** exhibited a binding energy of −6.99 kcal/mol against Bcl-2. It interacted with Arg146 by one H-bond with a distance of 2.62 Å, additionally, it interacted with Ala149, Phe104, Arg146, and Leu137 by three *pi*-alkyl interactions (*Supplementary Figure 5F*).

Density Functional Theory (DFT) Study

DFT parameters, including total energy,[37] HOMO,[37] LUMO,[37] gap energy,[38] and dipole moment,[39,40] were studied using the Discovery Studio 2019 Software, and the co-crystallized ligand **colchicine** was used as a reference molecule.

The total energies of the synthesized compounds and **colchicine** were calculated and presented in *Supplementary Table 3*. Compounds **3**, **5**, **6**, **8**, and **colchicine** showed the highest energies: −2664.98, −2986.98, −5098.91, −2566.57, and −1347.80 kcal/mol, respectively. These results indicate that these compounds (compounds **3**, **5**, **6**, **8**) have higher total energy than **colchicine** and the other **CA-4** analogs and are expected to have a more efficient interaction with colchicine-binding site on β-tubulin. Furthermore, the dipole moment values of compounds **3**, **5**, **6**, **7**, and **colchicine** were 2.751, 3.648, 3.568, 3.148, and 1.714, respectively (*Supplementary Table 3*). These values suggest that the dipole moment of the mentioned compounds is greater than that of the other **CA-4** analogs and **colchicine**. In light of these findings, it was predicted that compounds **3** and **5** could conveniently form hydrogen bonds and non-bonded interactions with the colchicine-binding pocket in tubulin, resulting in an increased binding affinity during tubulin inhibition. Compound **3** had a gap energy value of 0.078 kcal/mol, denoting that it is more stable than other compounds. As a result, compound **3** was thought to be the most likely candidate for interacting with the target protein tubulin. The HOMO and LUMO properties play critical roles in chemical stability and reactivity (*Supplementary Figure 6*).[40] Compound **3** had HOMO and LUMO values of −0.14419 and −0.06583, respectively, indicating that it has an excellent distribution of electron density around all of its atoms, and that it binds with strong attraction and hydrogen bonds.

Molecular Similarity

Supplementary Table 4 displays the computed molecular similarity between the newly synthesized compounds, and the reference ligand **colchicine**. The extent of molecular similarity or likeness between two compounds is represented by a similarity coefficient, which is used to compute a quantitative scoring rate. This calculated score reflects the degree of similarity and is based on the values of several structural descriptors. The calculated distance between two compounds in descriptor space is inversely proportional to their similarity.[41] The distances between the various descriptors were calculated in this study (*Supplementary Figure 7*). Among the evaluated compounds, the molecular similarity study preferred four compounds: **1**, **2**, **3**, and **7** with strong similarity to the reference compound **colchicine**.

ADMET Studies

Using the Discovery Studio 2019 Software and **colchicine** as a reference drug, ADMET analyses were performed (*Supplementary Figure 8* and *Supplementary Table 5*). The blood-brain barrier penetration levels for the newly synthesized **CA-4** analogs ranged from low to very low, and **colchicine** and compounds **1**, **2**, and **3** were found to have excellent absorption properties. Furthermore, the solubility levels of the synthesized compounds were anticipated to be low to very low compared to that of **colchicine** (good). All of the molecules tested, including **colchicine**, were predicted to be non-

inhibitors of CYP2D6. Hepatotoxicity assumptions revealed that all of the tested compounds were predicted to be non-toxic, and that all of the newly synthesized compounds, with the exception of compounds **6** and **colchicine**, were presumed to bind to plasma proteins more than 90% of the time (*Supplementary Figure 8* and *Supplementary Table 5*).

MD Simulation Studies

To detect the stability of the protein (tubulin)-ligand (the new **CA-4** analogs) complex in the apo and ligand bonded states, the dynamic movements of atoms and conformational variations of backbone atoms were determined by calculating the root mean square deviation (RMSD) for compounds **3** and **5** (*Figure 4 and Supplementary Figure 9*, respectively). The protein, ligand, and complex have lower RMSD with no significant fluctuations, implying greater stability. The flexibility of each residue was computed in terms of root mean square fluctuation (RMSF) to gain a deeper understanding of the protein areas that fluctuated during the simulation. It was obvious that the binding of the ligand makes β-tubulin a little flexible. The radius of gyration (Rg) symbolized the complex's compactness. The lower the degree of fluctuation over the simulation period, the more compact the system. The complex's Rg was observed to be almost identical to the starting period for compound **3**, while it was slightly higher than the starting period for compound **5**. Over the simulation period, the interaction between protein-ligand complexes and solvents was measured using solvent accessible surface area (SASA). As a result, the complex's SASA was estimated to determine the extent of the conformational changes that occurred during the interaction. Surprisingly, the protein showed a decrease in surface area with a lower SASA value than the starting period. Hydrogen bonding between protein-ligand complexes is necessary for structure stability. The protein formed up to two hydrogen bonds with the ligand in the greatest number of conformations.

Based on these results, compound **3** has a good dynamic profile (*Figure 4*), as indicated by a lower Rg value than the starting period which suggesting that compound **3** fitted appropriately with the targeted protein (β-tubulin) and has low number of conformational changes, although no more major fluctuation was noted. Compound **3** showed lower RMSD value at 100 ns time of simulation with lower SASA value than the starting period. It can form 1–2 hydrogen bonds with total energy of −1263 KJ/mol with the protein. On the other hand, compound **5** has low RMSD value at 100 ns time of simulation with lower SASA value than the stating period (*Supplementary Figure 9*). There were some minor fluctuations with low Rg, and compound **5** can form 1–2 hydrogen bonds with total energy −1049 KJ/mol with the protein.

*Molecular-Mechanics Poisson-Boltzmann Surface Area (MM/PBSA) of Compounds **3** and **5***

We calculated the binding free energy of the last 20 ns of MD simulation run of the protein-ligand complex with an interval of 100 ps from MD trajectories using MM/PBSA method. We also utilized the MmPbSaStat.py script that calculated the average free binding energy and its standard deviation/error from the output files that were obtained from MM/PBSA. Compounds **3** (*Supplementary Figure 10A*), and **5** (*Supplementary Figure 10C*) showed the lowest binding free energy of −1263 KJ/mol, and −1049KJ/mol, respectively. Furthermore, we identified the contribution of each residue of the protein in terms of the binding free energy. This gave us an insight into the 'crucial' residues that contributes favorably to the binding of the compounds to human tubulin. It was found that for compound **3**, Asp69, Glu71, Glu77, Asp98, and Glu183 residues in α-tubulin, and Asp251 and Asp329 residues in β-tubulin contributed higher than −40 KJ/mol binding energy (*Supplementary Figure 10B*). For compound **5**, it was found that Asp69, Glu71, Asp76, Glu77, Asp98, and Glu183 residues in α-tubulin, and Glu327, Glu330, and Asp357 residues in β-tubulin contributed higher than −40 KJ/mol binding energy (*Supplementary Figure 10D*). Therefore, these residues are hotspot residues in binding of human tubulin with compounds **3** and **5**.

3D-QSAR Model Validation

Ten FDA approved tubulin inhibitors were used for the generation of the 3D-QSAR model. The model shows R^2 value of 0.937 indicating it is a valid model. Additionally, the predicted and experimental data (predicted PIC_{50} and experimental PIC_{50}) for the FDA-approved tubulin inhibitors (*Supplementary Table 6*), indicate the validation of the model to evaluate the new **CA-4** analogs (*Supplementary Figure 11*). Compounds **3**, **5**, **6**, and **9** showed excellent predicted PIC_{50} (−0.713, −0.483, 0.873, and −0.779, respectively) compared to the experimental PIC_{50} (−0.802, −0.820, −1.278, −1.079, respectively) (*Supplementary Table 6*). Compounds **1**, **2**, and **4** showed comparable values of

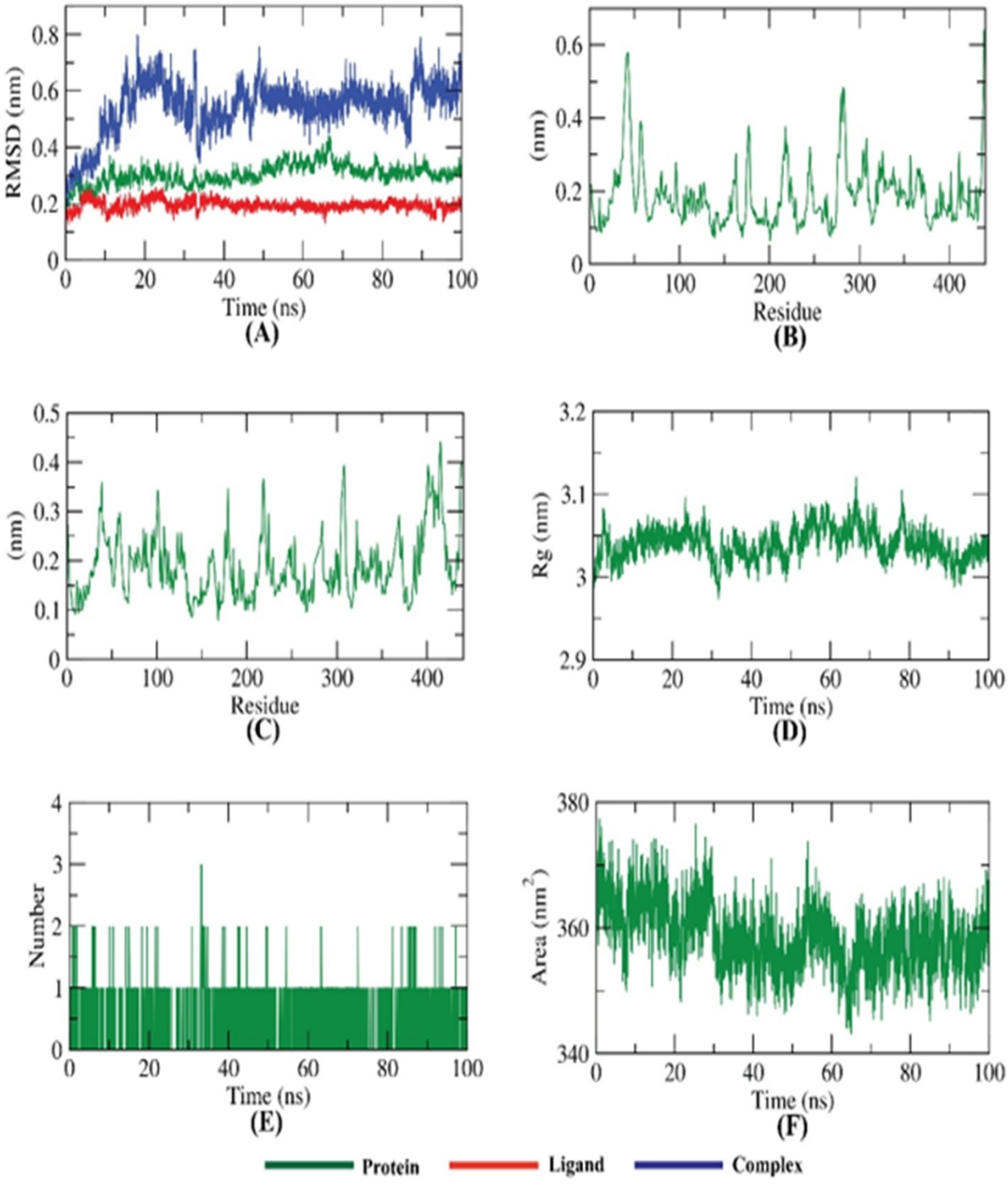

Figure 4. MD simulation trajectory analysis of compound **3**. A) Root Mean Square Divisions (RMSD), B and C) Root Mean Square Fluctuations (RMSF), D) Radius of gyration (Rg), E) Number of H-bond, F) Solvent accessible surface area plot.

predicted PIC_{50} (−0.487, −0.509, and 0.478, respectively) compared to the experimental PIC_{50} (−1.238, −1.447, and −1.724, respectively) (*Supplementary Table 7*), while compounds **7** and **8** failed to show close predicted PIC_{50} (−0.470 and −0.497, respectively) to the experimental PIC_{50} (−1.740 and −1.311, respectively) (*Supplementary Table 7*).

Evaluation of Biological Activity

Cytotoxicity Assay

The results of the docking studies presented in the current study indicated that the newly synthesized **CA-4** analogs target microtubules, the cytoskeleton element needed for chromosome segregation, leading to disruption in cell division and proliferation. To confirm these results, the *in vitro* anti-proliferation activity of the novel analogs was investigated by means of the MTT assay. The results presented in *Table 1* show that all compounds exhibit cytotoxicity against the three cancer cell lines tested (Hep G2, HCT-116, and A549), they are more cytotoxic to the liver cancer cell line Hep G2 than the other two cell lines, and that compound **3** is the most cytotoxic compound resulting in the lowest IC_{50} value (6.35 μM against Hep G2 liver cancer cells), a very close value to that of the microtubule targeting drug **colchicine**[42] (2.51 μM).

To investigate the cancer-selectivity of compound **3** against cancer cells, normal cells (WI-38 normal lung fibroblasts) were treated and assayed by the MTT assay. The IC_{50} concentration of compound **3** against WI-38 cells was found to be 29.8 μM, giving a selectivity index (SI) of 4.7 (SI=IC_{50} normal cells/IC_{50} cancer cells).[43] A cancer-selective compound should have an SI value of ≥ 3, making compound **3** a cancer cytotoxic-selective agent.[44]

Compound **3** *Arrests Cells at the G2/M Cell Cycle Phase which Induces Apoptosis*

Since the results of the docking studies indicated that the newly synthesized compounds target microtubules, we aimed to confirm this by analyzing the distribution of cells during the different phases of the cell cycle. As expected, compound **3**-treated Hep G2 hepatocarcinoma cells were arrested at the G2/M phase, as a result of targeting the mitotic spindle fiber (*Figure 5*), similar results were reported previously for **colchicine**.[45] Moreover, the mechanism by which compound **3** exerted its cytotoxicity was investigated by staining vehicle (0.2% DMSO)-treated control and compound **3**-treated Hep G2 cells with Annexin V-FITC followed by flow cytometric analysis (*Table 2*). *Table 2* shows that compound **3** caused cytotoxicity in Hep G2 hepatocarcinoma cells by inducing apoptosis.

Compound **3** *Inhibits Microtubule Polymerization by Binding to Colchicine-Binding Site On β-Tubulin*

The three compounds with the lowest IC_{50} values, compounds **3**, **5**, and **9** (*Table 1*), were tested for their

Table 1. *In vitro* cytotoxicity results of the new **combretastatin** analogs against human liver (Hep G2), colorectal (HCT-116), and lung (A549) cancer cell lines, treated for 72 h. Results are shown as mean ± SEM of three independent experiments.

Compound	*In vitro* cytotoxicity IC_{50} (μM)			
	Hep G2	HCT-116	A549	WI-38
Colchicine	2.51 ± 0.30	4.16 ± 0.38	5.22 ± 0.42	7.74 ± 1.85
1	68.95 ± 3.17	52.85 ± 4.20	141.10 ± 5.89	–
2	28.03 ± 1.69	51.28 ± 6.62	36.17 ± 2.43	–
3	6.35 ± 1.05	9.21 ± 1.36	12.11 ± 1.09	29.80 ± 1.42
4	53.02 ± 3.77	105.40 ± 6.88	142.40 ± 9.95	–
5	6.62 ± 1.85	20.43 ± 2.96	14.37 ± 1.38	–
6	19.39 ± 1.36	20.84 ± 3.35	21.85 ± 1.97	–
7	55.07 ± 3.52	159.60 ± 6.85	116.90 ± 6.31	–
8	20.47 ± 1.89	31.84 ± 2.89	30.36 ± 2.87	–
9	12.01 ± 2.35	28.79 ± 1.63	17.72 ± 1.28	–

Table 2. Compound **3** causes cytotoxicity by inducing apoptosis in Hep G2 liver cancer cells. Values are given as mean ± SEM of two independent experiments.

Treatment	Viable	Apoptosis		Necrosis
		Early	Late	
Control	95.64 ± 1.46	1.40 ± 0.05	2.27 ± 1.05	0.69 ± 0.44
Compound 3	67.37 ± 4.99	9.54 ± 3.52	20.10 ± 3.52*	2.99 ± 0.55

*$p < 0.05$.

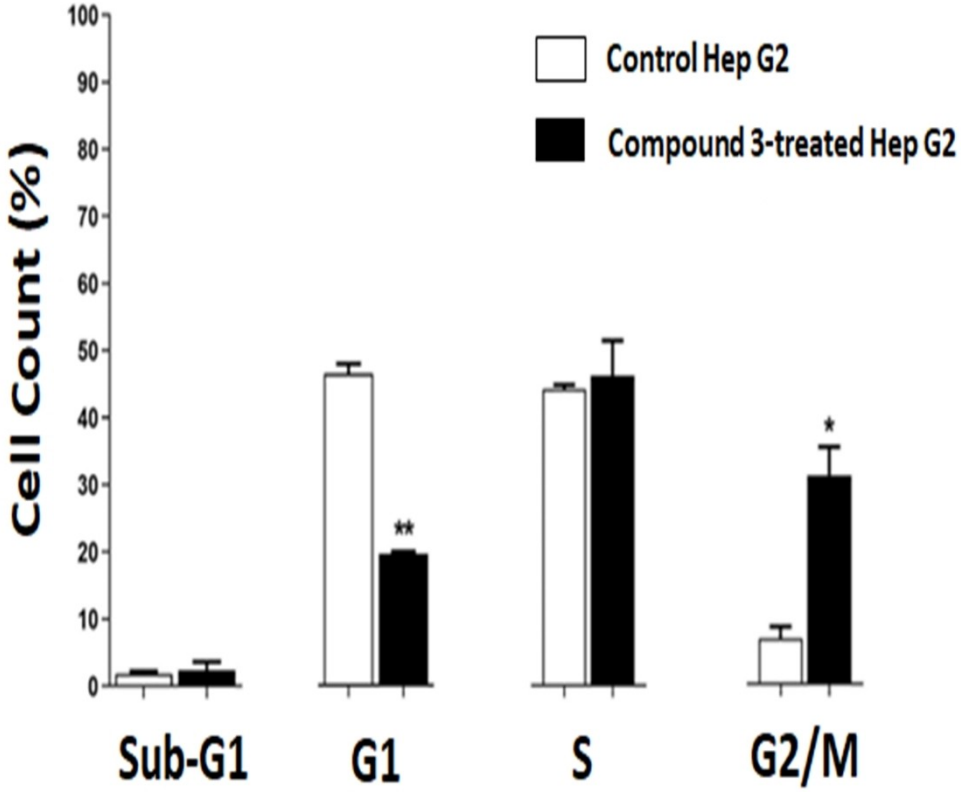

Figure 5. Effects of compound **3** on cell cycle progression. Hep G2 liver cancer cells were treated with 6.35 μM (IC_{50} value) of compound **3** for 72 h. Vehicle-treated (0.2% DMSO) control and compound **3**-treated cells were analyzed for their distribution (percentage) during the various phases of the cell cycle. Values are given as mean ± SEM of two independent experiments. *$p < 0.05$, **$p < 0.01$ as compared to control cells.

ability to inhibit microtubule polymerization by comparing them to the standard microtubule polymerization targeting drug **colchicine**.[42] 0.2% DMSO was used as vehicle control, and it had no effect on spontaneous tubulin self-assembly (*Figure 6A*). The results presented in *Figure 6B* and *Table 3* show that compound **3** tubulin polymerization IC_{50} (concentration of drug to inhibit 50% of tubulin assembly) was comparable to that of **colchicine** (9.50 μM and 5.49 μM, respectively). Additionally, compound **3** was able to reduce the Vmax of tubulin polymerization in a comparable fashion to that of **colchicine**, while compounds **5** and **9** were less successful (*Figure 6B*).

Table 3. Inhibition of tubulin polymerization (IC_{50}) of the tested compounds. Data are presented as mean ± SEM of three different experiments.

Compound	Tubulin polymerization IC_{50} (μM)
Colchicine	5.49 ± 0.85
3	9.50 ± 1.29
5	13.46 ± 1.17
9	35.20 ± 1.35

To investigate whether the newly synthesized **CA-4** analogs bind to colchicine-binding site on tubulin heterodimer, β-tubulin specifically,[44] the effects of these compounds on **colchicine** binding to tubulin was tested and compared to the positive control **CA-4**, and to the negative control **vinblastine** (*Figure 6C*). The results show that all compounds at 10 μM were able to inhibit **colchicine** binding to tubulin except for **vinblastine**, **CA-4** being the most potent, followed by compound **3**. At 50 μM, the inhibitory activities of compounds **3**, **5**, and **9** were enhanced (*Table 4*). These results indicate that the newly synthesized **CA-4** analogs bind tubulin at the colchicine binding site.

Structure-Activity Relationship (SAR)

The SAR presented in *Figure 7* is based on the results of the *in vitro* cytotoxic activities of the synthesized compounds. The effect of ring **B** (linker region) modifications on the activity were explored. Com-

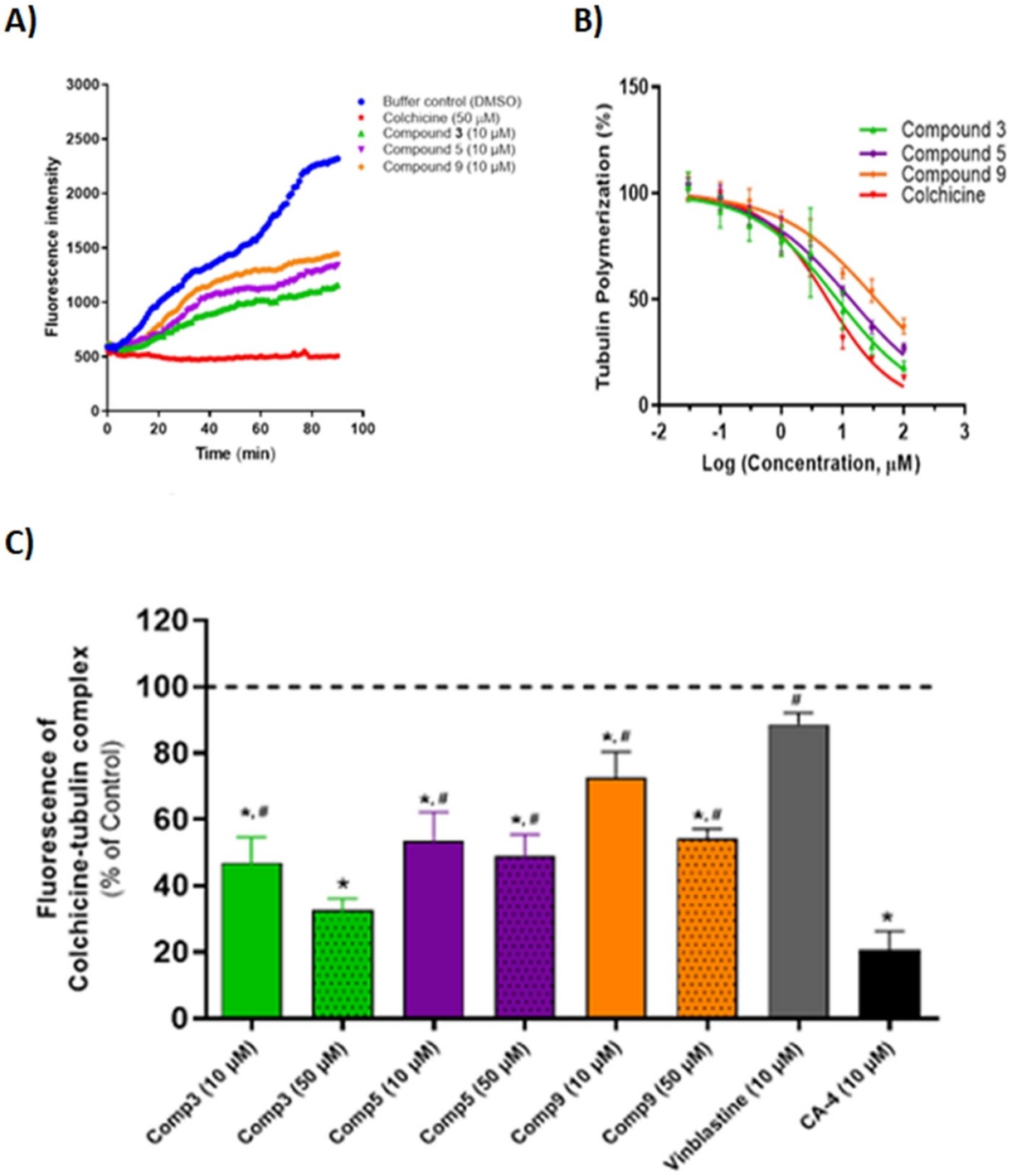

Figure 6. Effect of compounds **3**, **5**, and **9** on tubulin polymerization and **colchicine** binding to tubulin. A) *In vitro* polymerization of tubulin was monitored continuously by recording the fluorescence 1 min interval for 90 min. The fluorescence intensity curves represent average of at least three independent experiments, B) Inhibition of tubulin polymerization after treating with different concentrations of the tested compound and **colchicine**. IC_{50} values were calculated from data at the 30 min time point at 37 °C, C) Percentage fluorescence of **colchicine**-tubulin complex. Fluorescence values are normalized to 0.2% DMSO (control). **CA-4** and **vinblastine** were used as positive and negative controls, respectively. Data are expressed as mean ± SEM of three independent experiments. * $p < 0.05$ as compared to control cells, # $p < 0.05$ as compared to **CA-4**-treated cells.

Table 4. Effect of the tested compounds on **colchicine** binding to tubulin. Data are presented as mean ± SEM of three independent experiments.

Compound	Inhibition of colchicine binding (%)	
	10 μM	50 μM
Vinblastine	11.40 ± 3.51	–
CA-4	79.24 ± 5.64	–
3	52.98 ± 7.64	67.19 ± 3.38
5	46.49 ± 8.77	51.14 ± 6.63
9	27.49 ± 7.96	45.88 ± 3.09

pound **3** with terminal pyrrolidine moiety attached to the substituted triazole (ring **B**) was the most potent cytotoxic compound (lowest IC_{50} = 6.35 μM), while the order of cytotoxicity for the rest of the triazole substituents was as follow: compound **5** (4-chloro phenyl substituent) > compound **9** (unsubstituted phenyl attached to triazole) > compound **6** (4-bromo phenyl substituent) > compound **8** (4-methoxy phenyl attached to triazole) > compound **2** (5-methyl-1,2-dihydro-3*H*-pyrazol-3-one ring) > compound **4** (4-methoxy phenyl substituent) > compound **7** (unsubstituted phenyl hydrazine-1-carbothioamide ring) > compound **1** (carbohydrazide attached to triazole moiety). Regarding the substituted triazole five membered ring **B**, it was found that cytotoxicity increases with hydrophobic moiety added at the terminal substituent attached to the triazole ring, more than the hydrophilic unsubstituted moiety.

Conclusions

A New series of nine **combretastatin A4** (**CA-4**) analogs were effectively synthesized and validated by FT-IR, ^{1}H-NMR, ^{13}CNMR, and HR-MS techniques. *In silico* analysis indicated that compound **3** has higher total energy and dipole moment than other compounds and **colchicine**, it has excellent distribution of electron density and is more stable, resulting in an increased binding affinity during tubulin inhibition. As a result, compound **3** was thought to be the most likely candidate for interacting with the target protein tubulin. Additionally, compound **3** was found to interact with three apoptotic markers, namely p53, Bcl-2, and caspase 3. Among the evaluated **CA-4** analogs, the molecular similarity study preferred four compounds (**1**, **2**, **3**, and **7**) with strong similarities to the reference compound **colchicine**. Compound **3** has excellent pharmacokinetics properties, and a good dynamic profile. Moreover, the *in vitro* studies showed that all compounds exhibit cytotoxicity against the three cancer cell lines tested (Hep G2, HCT-116, and A549), they are more cytotoxic to the liver cancer cell line Hep G2, and that compound **3** is the most cytotoxic, and based on its SI, compound **3** is a cancer cytotoxic-selective agent. As expected and similar to

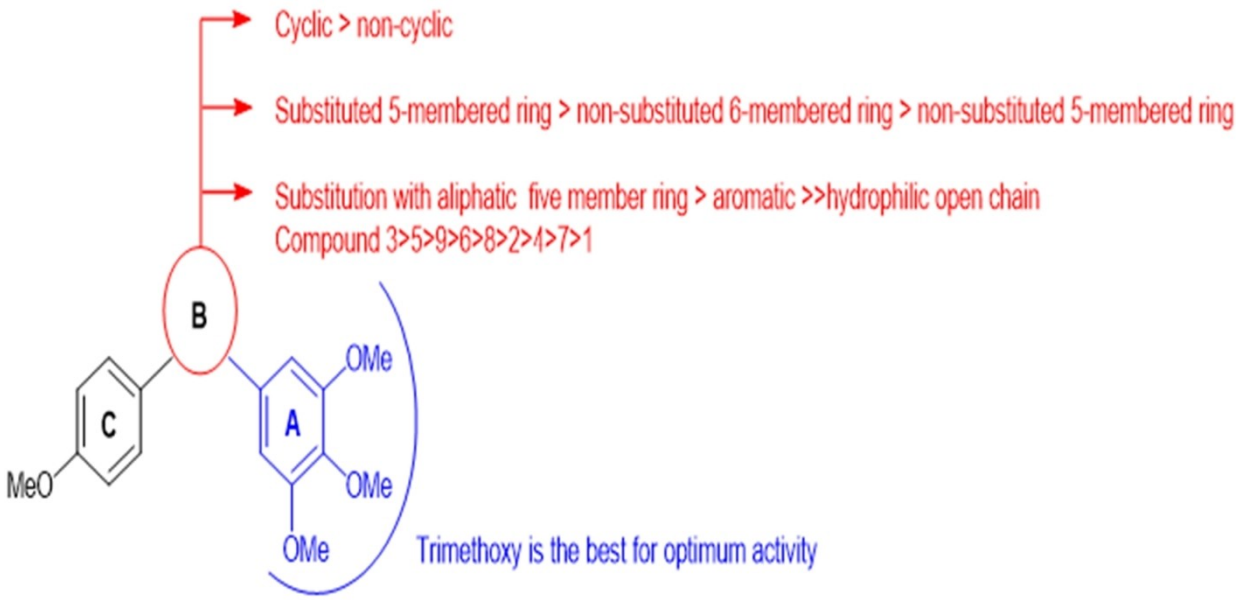

Figure 7. Structure-activity relationship of the newly synthesized **CA-4** analogs as anti-proliferative agents.

colchicine, compound **3**-treated Hep G2 hepatocarcinoma cells were arrested at the G2/M phase, as a result of targeting the mitotic spindle fiber. Compound **3** caused cytotoxicity in Hep G2 hepatocarcinoma cells by inducing apoptosis, and its tubulin polymerization IC_{50} (concentration of drug to inhibit 50% of tubulin assembly) and effect on V_{max} of tubulin polymerization was comparable to that of **colchicine**. Additionally, compound **3** binds tubulin at the colchicine-binding site. Taken together, the findings of the current study suggest that compound **3** is a promising microtubule-disrupting agent with excellent potential to be used as cancer therapeutic agent.

Experimental Section

Chemistry

General

All of the chemicals and reagents used were purchased from Baoji Guokang Bio-Technology and used as received without any further purification. Compounds **S1** and **S2** were synthesized according to previous reports.[33] The ^{1}H-NMR spectra were recorded on Bruker (BioSpin 400 MHz) spectrometer, chemical shift values δ (ppm) were reported to tetramethylsilane (TMS), as an internal reference, CD_2Cl_2 and $DMSO_{d6}$ were used as solvents. FT-IR spectra were measured on a Tensor II, Bruker-Optics FT-IR spectrophotometer, as KBr disc. Mass spectra were recorded on API 3200 quadruple, ESI system (Applied Biosystem) mass spectrometer.

Synthesis of 2-((4-(4-methoxyphenyl)-5-(3,4,5-trimethoxyphenyl)-4H-1,2,4-triazol-3-yl)thio)acetohydrazide (**1**)[34]

Compound **S2** (4 g, 9.0 mmol) was dissolved in abs EtOH (40 mL), an excess amount of 80% hydrazine hydrate solution (5 ml) was added, and the reaction mixture was refluxed for 12 h. The reaction was then cooled to room temperature (RT), the solid product was collected by filtration, washed with diethyl ether, and recrystallized from EtOH to yield compound **1**.

White crystals. Yield: 66%, R_f = 0.2 (hexane/ethylacetate8 : 2). m.p.: 181–183 °C. FT-IR (KBr disc, cm^{-1}) 3307 and 3141 (NH_2) str, 3224 (NH) str, 3075, 3060 and 3003 (Ar–H), 2970, 2937 and 2831 (–C–H) str., 1671 (C=O) str, 1607 (C=N) str, 1586, 1512, 1485 (Ar–C=C) str, 1249 and 1228 (Ar-C-O), 1181 (C–N) str. ^{1}HNMR (400 MHz, $DMSO_{d6}$; δ, ppm) 9.34 (s, 1H, NH), 7.38 (d, J = 8.8Hz, 2H, Ar–H), 7.11 (d, J = 8.8Hz, 2H, Ar –H), 6.66 (s, 2H, Ar.–H), 4.30 (s, 2H, NH_2), 3.88 (s, 3H, O–CH_3), 3.83 (s, 2H, S–CH_2), 3.63 (s, 3H, O–CH_3). ^{13}C-NMR (100 MHz, $DMSO_{d6}$; δ, ppm): 166.54 (C=O), 160.65 (Ar–C), 154.66, 153.07, 152.26, 138.91, 129.68, 126.81, 122.22, 115.52, 105.76 (Ar–C), 60.51 (OCH_3), 56.10 (OCH_3), 56.07 (OCH_3), 34.62 (CH_2). MS (ESI) *m/z*: calcd. for $C_{20}H_{23}N_5O_5S$ $[M+1]^+$ 446.15, found 446.4.

Synthesis of 1-(2-((4-(4-methoxyphenyl)-5-(3,4,5-trimethoxyphenyl)-4H-1,2,4-triazol-3-yl)thio)acetyl)-5-methyl-1,2-dihydro-3H-pyrazol-3-one (**2**)[34]

Compound **1** (0.5 g, 1.12 mmol) was dissolved in abs EtOH (30 mL), ethyl acetoacetate (0.145 ml, 0.145 g, 1.12 mmol) was added, the mixture was refluxed for 8 h, then the solvent was evaporated under reduced pressure, the solid product was washed with diethyl ether, and recrystallized from acetone to yield compound **2**.

Brown solid. 3200 (NH) str, 3112, 3070 (Ar–H), 2998, 2935, 2837 (C–H) str, 1736 (C=O) str, 1677 (amide, C=O) str, 1608 (C=N) str, 1587, 1515, and 1485 (ArC=C) str, 1266 and 1252 (Ar–C–O) str, 1199 (C–N) str. ^{1}HNMR (400 MHz, CD_2Cl_2; δ, ppm): 11.36 (s, 1H, NH), 7.26 (d, J = 8.70Hz, 2H, Ar–H), 7.08 (d, J = 8.43Hz, 2H, Ar–H), 6.69 (d, 2H, Ar–H), 4.47 (s, 1H, C=C–H), 4.19 (S, 2H, S–CH_2), 3.90–3.79 (m, 9H, O–CH_3), 3.66 (s, 3H, O–CH_3), 2.15 (s, 3H, CH_3). ^{13}CNMR (100 MHz, CD_2Cl_2; δ, ppm):166.54 (C=O), 160.66 (Ar–C), 154.58, 153.09, 152.28, 138.98, 129.71, 126.80, 126.62, 122.30, 115.53, 105.77 (Ar–C), 100.18 (CH=C), 61.76 (OCH_3), 60.96, 60.53, 56.11 (OCH_3), 44.42 (S–CH_2), 44.33, 17.26 (CH_3). MS (ESI) *m/z*: calcd. for $C_{24}H_{25}N_5O_6S$ $[M+1]^+$ 512.15, found 512.3.

Synthesis of 2-((4-(4-methoxyphenyl)-5-(3,4,5-trimethoxyphenyl)-4H-1,2,4-triazol-3-yl) thio)-N-(pyrrolidin-1-yl)acetamide (**3**)[34]

In a mixture of glacial acetic acid (GAA) (10 mL), and tetrahydrofuran (THF) (5 mL), compound **1** (0.5 g, 1.12 mmol) was dissolved, and stirred at RT for 1 h, then the mixture was refluxed for 8 h. After cooling to RT, the solvent was reduced to half (under reduced pressure), and poured over crushed ice, off-white solid was precipitated, filtered, and recrystallized from EtOH to give compound **3**.

Off white powder. Yield: 49%. R_f = 31(hexane/ethyl acetate 8:2). m.p.: 201–203 °C. FT-IR (KBr disk, cm^{-1}): 3204 (NH) str, 2997, 2961, 2837 (C–H) str, 1672 (C=O) str, 1606 (C=N) str, 1586, 1510, 1459 (ArC=C) str, 1244 (Ar–C–O) str, 1029 (C–N) str. ^{1}H-NMR (400 MHz, CD_2Cl_2; δ, ppm): 10.31 (s, 1H, NH), 7.28 (d, 2H, ArH), 7.07 (d, 2H, ArH), 6.70 (s, 1H, Ar–H), 3.96 (s, 2H, S–CH_2), 3.88 (s, 3H, OCH_3), 3.79 (s, 3H, OCH_3), 3.65 (s, 6H, 2x OCH_3), 2.14–1.96 (m, 8H, 4x CH_2-pyrollidine). ^{13}C-NMR (100 MHz, CD_2Cl_2; δ, ppm): 167.84 (C=O), 166.53 (Ar–C), 166.18, 161.31, 155.39, 153.80, 153.57, 129.11, 126.64, 121.77, 115.64, 105.72 (Ar–C), 60.82 (OCH_3), 56.24 (OCH_3), 56.10 (OCH_3), 33.85 (S–CH_2), 20.99 (CH_2). MS (ESI) *m/z*: calcd. for $C_{24}H_{29}N_5O_5S$ $[M]^+$ 499.19, found 499.5.

General Procedure for Synthesis of Compounds **4–7**[35]

In abs EtOH (20 mL), compound **1** (0.1g, 0.225 mmol), and the appropriate phenyl isothiocyanate (0.225 mmol): a: 4-methoxy phenyl isothiocyanate (0.137g); b: 4-chlorophenyl isothiocyanate (0.138g); c: 4-bromophenyl isothiocyanate (0.148g), d: phenyl isothiocyanate (0.130 g), was separately dissolved, and stirred for 6 h at 40–55 °C to produce the new analogs (**4**–**7**, respectively) which were separated by filtration, washed with diethyl ether, and recrystallized from EtOH (75%).

N-(4-methoxyphenyl)-2-(2-((4-(4-methoxyphenyl)-5-(3,4,5-trimethoxyphenyl)-4H-1,2,4-triazol-3-yl)thio)acetyl)hydrazine-1-carbothioamide (*4*). White powder. Yield: 67%. R_f = 0.34 (hexane/ethylacetate8:2). m.p.: 199–201 °C. FT-IR (KBr disc, cm^{-1}): 3288 (Ar–H) str, 3218 (*H–N–*C=S) str, 3151 (*H–N–*C=O) str, 2980 2935, 2837 (C–H) str, 1704 (C=O) str, 1586, 1541, 1486 Ar(C=C) str, 1249, 1233 (Ar–C–O) str, 1189 (C=S) str, 1080 (C–N) str. ^{1}H-NMR (400 MHz, $DMSO_{d6}$; δ, ppm): 10.40 (s, 1H, NH), 9.66 (s, 2H, NH), 7.41 (d, 2H, Ar–H), 7.35 (d, 2H, Ar–H), 7.13 (d, *J* = 8.5, 2H, Ar–H), 6.89 (d, *J* = 8.4, 2H, Ar–H), 6.60 (s, 2H, Ar–H), 3.97 (s, 2H, S–CH_2), 3.81 (s, 3H, OCH_3), 3.72 (s, 3H, OCH_3), 3.63 (s, 3H, OCH_3), 3.33 (s, 3H, OCH_3). ^{13}C-NMR (100 MHz, $DMSO_{d6}$; δ, ppm):) 160.73 (Ar–C), 157.24, 154.53, 153.07, 152.49, 138.99, 132.26, 129.68, 126.69, 122.04, 115.60, 113.57, 105.67 (Ar–C), 60.53 (OCH_3), 56.10 (OCH_3), 56.09 (OCH_3), 55.63 (OCH_3), 34.74 (CH_2). MS (ESI) *m/z*: calcd. for $C_{28}H_{30}N_6O_6S_2$ $[M+1]^+$ 611.17, found 611.30.

N-(4-chlorophenyl)-2-(2-((4-(4-methoxyphenyl)-5-(3,4,5-trimethoxyphenyl)-4H-1,2,4-triazol-3-yl)thio)acetyl)hydrazine-1-carbothioamide (*5*). White powder. Yield: 43%, R_f = 0.37 (hexane/ethylacetate8:2). m.p.: 210–213 °C. FT-IR (KBr, cm^{-1}): 3300 (Ar–NH) str, 3161 (*H–N–*C=S) and (*H–N–*C=O) str, 2959 and 2836 (CH_3) str, 1712 (C=O) str, 1609 (C=N) str, 1586, 1537, and 1512 (ArC=C) str, 1232 (Ar–C–O), 1192 (C=S) str, 1072 (C–N) str. ^{1}H-NMR (400 MHz, $DMSO_{d6}$; δ, ppm): 10.47 (s, 1H, NH), 9.88 (s, 1H, NH), 9.83 (s, 1H, NH), 7.57–7.37 (m, 6H, Ar–H), 7.13 (d, *J* = 8.8, 2H, Ar–H), 6.65 (d, 2H, Ar–H), 3.96 (s, 2H, S–CH_2), 3.81 (s, 3H, OCH_3), 3.63 (s, 3H, OCH_3), 3.16–3.15 (s, 6H, 2x OCH_3). ^{13}C-NMR (100 MHz, $DMSO_{d6}$; δ, ppm): 181.00 (C=S), 160.75 (C=O), 160.69 (Ar–C), 154.53, 153.07, 139.00, 138.38, 129.69, 128.25, 126.65, 121.99, 115.60, 115.55, 105.64 (Ar–C), 60.52 (OCH_3), 56.07 (OCH_3), 49.05 (OCH_3), 34.67 (CH_2). MS (ESI) *m/z*: calc. for $C_{27}H_{27}ClN_6O_5S_2$ $[M+2]^+$ 615.12, found 615.6.d

N-(4-bromophenyl)-2-(2-((4-(4-methoxyphenyl)-5-(3,4,5-trimethoxyphenyl)-4H-1,2,4-triazol-3-yl)thio)acetyl)hydrazine-1-carbothioamide (*6*). White powder. Yield:38%. R_f = 0.29 (hexane/ethyl acetate 8:2). m.p.: 198–200 °C. FT-IR (KBr, cm^{-1}): 3300 (Ar–NH) str, 3161 (*H–N–*C=S) and (*H–N–*C=O) str, 2959, 2933(C-H) str, 1716 (C=O) str, 1609 (C=N) str, 1586, 1531, and 1485 (ArC=C) str, 1251 and 1232 (Ar–C–O) str, 1192 (C=S) str, 1072 (C–N) str. ^{1}H-NMR (400 MHz, $DMSO_{d6}$; δ, ppm): 10.48 (s, 1H,NH), 9.90 (s, 1H,NH), 9.83 (s, 1H,NH), 7.53–7.41 (m, 6H, Ar–H), 7.15 (d, 2H, Ar–H), 6.64 (d, 2H, A-rH). 3.97 (s, 2H, S–CH_2), 3.83–3.57 (m, 12H, 4x OCH_3). ^{13}C-NMR (100 MHz, $DMSO_{d6}$; δ, ppm): 180.65 (C=S), 166.87 (C=O), 160.19 (Ar–C), 153.97, 152.51, 152.00, 138.38, 138.23, 130.64, 129.14, 127.90, 126.08, 121.44, 117.37, 115.04, 105.02 (Ar–C), 59.96 (OCH_3), 55.51 (OCH_3), 34.10 (CH_2). MS (ESI) *m/z*: calcd. for $C_{27}H_{27}BrN_6O_5S_2$ $[M+3]^+$ 661.07, found 661.1.

2-(2-((4-(4-methoxyphenyl)-5-(3,4,5-trimethoxyphenyl)-4H-1,2,4-triazol-3-yl)thio)acetyl)-N-phenylhydrazine-1-carbothioamide (*7*). White powder. Yield: 61%. R_f = 0.23 (hexane/ethylacetate8:2). m.p.: 185–188 °C. FT-IR (KBr, cm^{-1}): 3299 (Ar–NH) str, 3194 (*H–N–*C=S) str, 3154 (*H–N–*C=O) str, 2973, 2836 (C–H) str, 1712 (C=O) str, 1610 (C=N) str, 1585, 1535, and 1485 (Ar–C=C) str, 1250 and 1231 (Ar–C–O) str, 1072 (C–N) str, 1199 (C=S) str. ^{1}H-NMR (400 MHz, $DMSO_{d6}$; δ, ppm): 10.44 (s, 1H, NH), 9.77 (s, H, NH), 9.76 (s,1H,NH), 7.55 (d, 2H, Ar–H), 7.41 (d, 2H, Ar–H), 7.32 (t, 2H, Ar–H), 7.17–7.11 (dd, 3H, Ar–H), 6.66 (s, 2H, Ar–H), 3.98 (s, 2H, S–CH_2), 3.81 (s, 3H, OCH_3), 3.64 (s, 3H,OCH_3), 3.55 (s, 6H, 2xOCH_3). ^{13}C-NMR (100 MHz, $DMSO_{d6}$; δ, ppm): 181.26 (C=S), 160.73 (C=O), 154.57 (Ar–C), 153.08, 152.48, 139.41, 138.99, 129.68, 128.37, 126.70, 125.57, 122.06, 115.59, 105.68 (Ar–C), 60.53 (OCH_3), 56.11

(OCH_3), 34.78 (CH_2). MS (ESI) *m/z*: calcd. for $C_{27}H_{28}N_6O_5S_2$ $[M]^+$ 580.16, found 580.59.

General Procedure for the Synthesis of Compounds **8** *and* **9**

Compound **4** (0.21g,0.344 mmol) or compound **7** (0.2g,0.344 mmol) was separately dissolved in aqueous solution of NaOH (25 ml, 2 N), and refluxed for 4 h, then the mixture was cooled and acidified by cold conc. HCl. The precipitates were collected by filtration, and washed thoroughly with D.W, and recrystallized from EtOH to yield the desired product.[36]

4-(4-methoxyphenyl)-5-(((4-(4-methoxyphenyl)-5-(3,4,5-trimethoxyphenyl)-4H-1,2,4-triazol-3-yl)thio)methyl)-4H-1,2,4-triazole-3-thiol (*8*). White powder. Yield: 71%. $R_f = 0.55$ (hexane/ethylacetate 8:2). m.p.: 207–209 °C. FT-IR (KBr, cm^{-1}): 3011 (Ar–H) str, 2964, 2934, 2837 (–C–H) str, 1607 (C=N) str, 1586, 1512, and 1484 (ArC=C) str, 1247 (Ar–C–O) str, 1123 (C–N) str. ^{1}H–NMR (400 MHz, $DMSO_{d6}$; δ, ppm): 13.80 (s, 1H, NH-thione *taut.*), 7.21–7.04 (m, 8H, Ar–H), 6.63 (s, 2H, Ar–H), 4.11 (s, 2H, S–CH_2), 3.81–3.79 (s, 6H, 2x OCH_3), 3.34 (s, 3H, OCH_3), 3.56 (s, 3H, OCH_3). ^{13}C-NMR (100 MHz, $DMSO_{d6}$; δ, ppm): 168.95 (C=S), 160.62(Ar–C), 160.22, 154.95, 153.08, 150.24, 149.03, 139.02, 129.97, 129.52, 126.73, 126.05, 122.04, 115.48, 114.93, 105.75 (Ar–C), 60.53 (OCH_3), 56.10 (OCH_3), 55.90 (OCH_3), 27.83 (CH_2). MS (ESI) *m/z*: calcd. for $C_{28}H_{28}N_6O_5S_2$ $[M]^+$ 593.16, found 593.3.

5-(((4-(4-methoxyphenyl)-5-(3,4,5-trimethoxyphenyl)-4H-1,2,4-triazol-3-yl)thio)methyl)-4-phenyl-4H-1,2,4-triazole-3-thiol (*9*). White powder. Yield: 56%. $R_f = 0.61$ (hexane/ethyl acetate 8:2). m.p.: 196–199 °C. FT-IR (KBr, cm^{-1}): 3011, 3003 (Ar–H) str, 2934 and 2837 (–C–H) str, 1607 (C=N) str, 1586, 1512, and 1484 (ArC=C) str, 1247 (O–CH_3) str, 1123 (C–N) str. ^{1}H-NMR (400 MHz, $DMSO_{d6}$; δ, ppm): 13.87 (s, 1H, NH-thione *taut.*), 7.53 (d, 3H, Ar–H), 7.32 (d, 2H, Ar–H), 7.22 (d,2H, Ar–H), 7.09 (d, 2H, Ar–H), 6.64 (s, 2H, Ar–H), 4.13 (s, 2H, S–CH_2), 3.81 (s, 3H, OCH_3), 3.64 (s, 3H, OCH_3), 3.37 (s, 3H,OCH_3). ^{13}C-NMR (100 MHz, $DMSO_{d6}$; δ, ppm): 168.72 (C=S), 160.62 (Ar–C), 154.99, 153.09, 150.25, 148.72, 139.04, 133.61, 130.08, 129.81, 129.53, 128.72, 126.72, 122.03, 115.49, 105.76 (Ar–C), 60.53 (OCH_3), 56.11 (OCH_3), 27.91 (CH_2). MS (ESI) *m/z*: calcd. for $C_{27}H_{26}N_6O_4S_2$ $[M+3]^+$ 565.15, found 565.40.

In silico *Studies*

Method of Docking Study

Preparation of the Targeted Protein Tubulin

The binding site of human tubulin was generated as described in Supplementary Information.[46]

Preparation of Tested Ligands

The 3D structures of the tested compounds were prepared as described in Supplementary Information.[47]

Molecular Docking

The proposed binding interactions, affinity, preferred orientation of each docking pose, and binding Free energy (ΔG) of the compounds tested with human tubulin are described in Supplementary Information.[48,49]

Validation of Molecular Docking

The docking study algorithm was validated as described in Supplementary Information.

Molecular Similarity

The molecular similarity descriptors were calculated for the tested compounds then compared to the reference compound (**colchicine**), using the Discovery Studio 2019 Software as described in Supplementary Information.

ADMET Studies

Colchicine was used as a reference drug (for the newly synthesized compounds) in ADMET studies using the Discovery Studio 2019 Software as described in Supplementary Information.

Toxicity Studies

The Discovery Studio 2019 Software was used to generate toxicity predictions for the newly synthesized molecules, as described in Supplementary Information.

MD Simulation Methodology

Molecular dynamics simulation of the protein-ligand complexes was performed using GROMACS 2021.1

version and Linux 5.4 package as described in Supplementary Information.

3D-QSAR (3 Dimensional-Quantitative Structure-Activity Relationship) Model Generation and Validation

The 3D-QSAR model was generated by GridBased-TempModel protocol in the Discovery Studio 2019 Software as described in Supplementary Information.

Biological Investigation

Cell Culture

Human A549 lung cancer cells, human Hep G2 hepatocyte carcinoma cells, human HCT-116 colorectal carcinoma cells, and human WI-38 normal lung fibroblast cell lines were maintained in their specific media (Gibco, USA) and supplemented with fetal bovine serum (Gibco, USA) according to ATCC. Trypsin-EDTA (Millipore-Merck, USA) was used for cell passaging. Cells were incubated in 5% CO_2, 100% humidity at 37 °C.

MTT in vitro *Anti-Proliferation Assay*

The MTT cytotoxicity assay was performed according to Mosmann, 1983.[50,51] The different compounds were diluted in 0.2% DMSO and 8 different concentrations for each compound were prepared (100, 30, 10, 3, 1, 0.3, 0.1, and 0.03 μM) in the specific growth medium.

Flow Cytometric Analysis of Control and Treated Hep G2 Hepatocyte Carcinoma Cells

Hep G2 hepatocyte carcinoma cells were treated with compound **3** (at the IC_{50} concentration) for 72 h, harvested, stained with Annexin-V/propidium iodide (PI), and analyzed for cell cycle phases (Cell Cycle Assay Kit; Elabscience Biotechnology, USA) and apoptosis (Annexin V-FITC apoptosis detection kit; Elabscience Biotechnology, USA) using the Flowing Software (Turku Bioscience).

Tubulin Polymerization Assay

Colchicine (50 μM), 0.2% DMSO as a vehicle control, and compounds **3**, **5**, and **9** (each at 10 μM) were tested for their effects on tubulin polymerization (Tubulin Polymerization Assay Kit, Cytoskeleton, USA). *In vitro* polymerization of tubulin was monitored continuously by recording the fluorescence at 1 min interval for 90 min, increasing relative fluorescence units is indicative of tubulin polymerization.

Colchicine Competitive Binding Assay

Vinblastine (10 μM), **CA-4** (10 μM), and compounds **3**, **5**, and **9** at 10 μM and 50 μM were incubated with 3 μM tubulin in the presence or absence of 3 μM **colchicine** for 30 min at 37 °C. Results are shown as percentage fluorescence of colchicine-tubulin complex. Fluorescence values were normalized to 0.2% DMSO (control).

Statistical Analysis

Values are given as mean ± SEM of three independent experiments. *$p < 0.05$ indicates statistically significant difference as compared to control untreated cells in unpaired *t*-tests using GraphPad Prism 8 software.

Acknowledgements

The authors thank the Department of Pharmaceutical Chemistry, College of Pharmacy, University of Baghdad, for providing the experimental facilities.

Conflict of Interest

The authors declare no conflict of interest.

Data Availability Statement

The data that support the findings of this study are available from the corresponding author upon reasonable request.

Author Contribution Statement

SAA and AAR contributed to study conception and design, SAA collected data, SAA, AAR, and LHT analyzed and interpreted the results, SAA, AAR, AAB, YSY, RAA, and LHT contributed to manuscript preparation. All authors reviewed the results and approved the final version of the manuscript.

References

[1] F. Bray, J. Ferlay, I. Soerjomataram, R. L. Siegel, L. A. Torre, A. Jemal, 'Global cancer statistics 2018: Globocan estimates of incidence and mortality worldwide for 36 cancers in 185 countries', *Ca-Cancer J. Clin.* **2018**, *68*, 394–424.

[2] L. A. Decosterd, N. Widmer, K. Zaman, E. Cardoso, T. Buclin, C. Csajka, 'Therapeutic drug monitoring of targeted anticancer therapy', *Biomark Med.* **2015**, *9*, 887–93.

[3] G. La Regina, A. Coluccia, V. Naccarato, R. Silvestri, 'Towards modern anticancer agents that interact with tubulin', *Eur. J. Pharm. Sci.* **2019**, *131*, 58–68.

[4] E. Stec-Martyna, M. Ponassi, M. Miele, S. Parodi, L Felli, C Rosano, 'Structural comparison of the interaction of tubulin with various ligands affecting microtubule dynamics', *Curr. Cancer Drug Targets* **2012**, *12*, 658–666.

[5] A. Devi Tangutur, D. Kumar, K. V. Krishna, S. Kantevari, 'Microtubule targeting agents as cancer chemotherapeutics: An overview of molecular hybrids as stabilizing and destabilizing agents', *Curr. Top. Med. Chem.* **2017**, *17*, 2523–2537.

[6] M. Kavallaris, 'Microtubules and resistance to tubulin-binding agents', *Nat. Rev. Cancer* **2010**, *10*, 194–204.

[7] S. K. Coulup, G. I. Georg, 'Revisiting microtubule targeting agents: A-tubulin and the pironetin binding site as unexplored targets for cancer therapeutics', *Bioorg. Med. Chem. Lett.* **2019**, *29*, 1865–1873.

[8] N. Vindya, N. Sharma, M Yadav, K. Ethiraj, 'Tubulins – the target for anticancer therapy', *Curr. Top. Med. Chem.* **2015**, *15*, 73–82.

[9] C. Dumontet, M. A. Jordan, ' Microtubule-binding agents: a dynamic field of cancer therapeutics', *Nat. Rev. Drug Discovery* **2010**, *9*, 790–803.

[10] S. Sharma, C. Kaur, A. Budhiraja, A. Nepali, K. Gupta, M. K. Saxena, A. K. Bedi, P. M. S. Bedi, 'Chalcone based azacarboline analogs as novel antitubulin agents: design, synthesis, biological evaluation and molecular modelling studies', *Eur. J. Med. Chem.* **2014**, *85*, 648–660.

[11] R. Kaur, G. Kaur, R. K. Gill, R. Soni, J. Bariwal, 'Recent developments in tubulin polymerization inhibitors: an overview', *Eur. J. Med. Chem.* **2014**, *87*, 89–124.

[12] S. N. A. Bukharie, G. B. Kumar, H. M. Revankar, H. L. Qin, 'Development of combretastatins as potent tubulin polymerization inhibitors', *Bioorg. Chem.* **2017**, *72*, 130–147.

[13] N. Naumova, R. Sachl, 'Regulation of cell death by mitochondrial transport systems of calcium and bcl-2 proteins', *Membranes* **2020**, *10*, 299.

[14] E. Thomas, V. Gopala Krishnan, M. Hegde, S. Kumar, S. S. Karki, S. C. Raghavan, B. Choudhary, 'A novel resveratrol based tubulin inhibitor induces mitotic arrest and activates apoptosis in cancer cells', *Sci. Rep.* **2016**, *6*, 34653.

[15] F. Naaz, M. R. Haider, S. Shafi, M. S. Yar, 'Anti-tubulin agents of natural origin: targeting taxol, vinca, and colchicine binding domains', *Eur. J. Med. Chem.* **2019**, *171*, 310–31.

[16] S. K. Gupta, P. Singh, V. Ali, M. Verma, 'Role of membrane embedded drug efflux abc transporters in the cancer chemotherapy', *Oncol. Rev.* **2020**, *14*, 448.

[17] K. E. Arnst, Y. Wang, Z. N. Lei, D. Hwang, G. Kumar, D. Ma, D. N. Parke, Q. Chen, J. Yang, S. W. White, T. N. Seagroves, Z. Chen, D. D. Miller, Wei Li, 'Colchicine binding site agent dj95 overcomes drug resistance and exhibits antitumor efficacy', *Mol. Pharmacol.* **2019**, *96*, 73–89.

[18] M. Zweifel, G. C. Jayson, N. Reed, R. Osborne, B. Hassan, J. Ledermann, G. Shreeves, L. Poupard, S.-P. Lu, J. Balkissoon, D. J. Chaplin, G. J. S. Rustin, 'Phase ii trial of combretastatinA4 phosphate, carboplatin, and paclitaxel in patients with platinum-resistant ovarian cancer', *Ann. Oncol.* **2011**, *22*, 2036–2041.

[19] W. Li, H. Sun, S. Xu, Z. Zhu, J. Xu, 'Tubulin inhibitors targeting the colchicine binding site: a perspective of privileged structures', *Future Med. Chem.* **2017**, *9*, 1765–1794.

[20] S. N. Baytas, 'Recent advances in combretastatin A-4 inspired inhibitors of tubulin plymerization: An update', *Curr. Med. Chem.* **2022**, *29*, 3557–3585.

[21] P. R. Kamath, Sunil D, A. A. Ajees, 'Synthesis of indole-quinoline-oxadiazoles: their anticancer potential and computational tubulin binding studies', *Res. Chem. Intermed.* **2016**, *42*, 5899–5914.

[22] I. Khelifi, T. Naret, D. Renko, A. Hamze, G. Bernadat, J. Bignon, C. Lenoir, J. Dubois, J. D. Brion, O. Provot, M. Alami, 'Design, synthesis and anticancer properties of isocombretaquinolines as potent tubulin assembly inhibitors', *Eur. J. Med. Chem.* **2017**, *127*, 1025–34.

[23] J. Seligman, C. Twelves, 'Tubulin: an example of targeted chemotherapy', *Future Med. Chem.* **2013**, *5*, 339–352.

[24] N. Piekus-Słomka, R. Mikstacka, J. Ronowicz, S. Sobiak, 'Hybrid *cis*-stilbene molecules: novel anticancer agents', *Int. J. Mol. Sci.* **2019**, *20*, 1300.

[25] B. C. Das, X. Y. Tang, P. Rogler, T. Evans, 'Design and synthesis of 3,5-disubstituted boron-containing 1,2,4-oxadiazoles as potential combretastatin a-4 (ca-4) analogs', *Tetrahedron Lett.* **2012**, *53*, 3947–3950.

[26] B. Biersack, K. Effenberger, R. Schobert, M. Ocker, 'Oxazole-bridged combretastatin an analogs with improved anticancer properties', *ChemMedChem* **2010**, *5*, 420–27.

[27] K. Mahal, B. Biersack, S. Schruefer, M. Resch, R. Ficner, R. Schobert, T. Mueller, 'Combretastatin a-4 derived 5-(1-methyl-4-phenyl-imidazol-5-yl)indoles with superior cytotoxic and anti-vascular effects on chemoresistant cancer cells and tumors', *Eur. J. Med. Chem.* **2016**, *118*, 9–20.

[28] A. A. Kubba, W. A. Shihab, N. N Al-Shawi, 'In silico and in vitro approach for design, synthesis, and anti-proliferative activity of novel derivatives of 5-(4-Aminophenyl)-4-substituted phenyl-2,4-dihydro-3H-1, 2, 4-triazole-3-thione', *Research J. Pharm. and Tech.* **2020**, *13*, 3329–3339.

[29] F. Schmitt, L. C. Gosch, A. Dittmer, M Rothemund, T Mueller, R. Schobert, B. Biersack, A. Volkamer, M. Höpfner, 'Oxazole-bridged combretastatin A-4 derivatives with tethered hydroxamic acids: structure(−)activity relations of new inhibitors of hdac and/or tubulin function', *Int. J. Mol. Sci.* **2019**, *20*, 283.

[30] L. Li, D. Quan, J. Chen, J. Ding, J. Zhao, L. Lv, J. Chen, 'Design, synthesis, and biological evaluation of 1-substituted-2-aryl imidazoles targeting tubulin polymerization as potential anticancer agents', *Eur. J. Med. Chem.* **2019**, *184*, 111732.

[31] T. S. Ibrahim, M. M. Hawwas, A. M. Malebari, E. S. Taher, A. M. Omar, N. M. O'Boyle, E. McLoughlin, Z. K. Abdel-Samii, Y. A. M. M. Elshaier, 'Potent quinoline-containing combre-

tastatin a-4 analogs: design, synthesis, antiproliferative, and anti-tubulin activity', *Pharmaceuticals* **2020**, *13*, 393.
[32] B. Biersack, K. Effenberger, R. Schobert, M. Ocker, 'Oxazole-bridged combretastatin A analogs with improved anti-cancer properties', *ChemMedChem* **2010**, *5*, 420–427.
[33] S. Al-Mansury, A. A. Balakit, F. F. Alkazaz, K. N. Madlum, R. A. Ghaleb, 'Synthesis and anti-colon cancer activity of 1,2,4-triazole derivatives with aliphatic S-substituents', *Orient. J. Chem.* **2019**, *35*, 77–84.
[34] S. A. Abdul Hussein, A. A. Kubba, 'Synthesis, characterization and antimicrobial activity of new 2,5-disubstituted-1,3,4-thiadiazole derivatives', *Der Pharma Chem.* **2015**, *79*, 250–260.
[35] Y. Yaseen, A. Kubba, W. Shihab, L. Tahtamouni, 'Synthesis, docking study, and structure-activity relationship of novel niflumic acid derivatives acting as anticancer agents by inhibiting VEGFR or EGFR tyrosine kinase activities', *Pharmacia* **2022**, *69*, 595–614.
[36] A. H. Abbas, A. A. Mahmood, L. H. Tahtamouni, Z. A. Al-Mazaydeh, M. S. Rammaha, F. Alsoubani, R. I. Al-bayati, 'A novel derivative of picolinic acid induces endoplasmic reticulum stress mediated apoptosis in human non-small cell lung cancer cells: synthesis, docking study and anticancer activity', *Pharmacia* **2021**, *68*, 679–692.
[37] H. S. Mohammed, V. D. Tripathi, A. A. Darghouth, M. Taif, 'Synthesis, characterization, DFT calculation and antimicrobial activity of Co (II) and Cu (II) complexes with azo dye', *J. Phys.* **2019**, *1294*, 052051.
[38] I. Fleming, 'Frontier orbitals and organic chemical reactions', Wiley, NJ, USA, 1977.
[39] M. El-Nahass, M. Kamel, A. El-Deeb, A. Atta, S. Huthaily, 'Ab initio HF, DFT and experimental (FT-IR) investigation of vibrational spectroscopy of PN, N-dimethylaminobenzylidenemalononitrile (DBM)', *Spectrochim. Acta Part A* **2011**, *79*, 443–450.
[40] J. I. Aihara, 'Correlation found between the HOMO-LUMO energy separation and the chemical reactivity at the most reactive site for isolated-pentagon isomers of fullerenes', *Phys. Chem. Chem. Phys.* **2000**, *2*, 3121–3125.
[41] R. G. Yousef, H. M. Sakr, I. H. Eissa, A. B. Mehany, A. M. Metwaly, M. A. Elhendawy, M. M. Radwan, M. A. ElSohly, H. S. Abulkhair, K. El-Adl, 'New quinoxaline-2 (1 H)-ones as potential VEGFR-2 inhibitors: design, synthesis, molecular docking, ADMET profile and anti-proliferative evaluations', *New J. of Chem.* **2021**, *36*, 16949–16964.
[42] E. W. Taylor, 'The mechanism of colchicine inhibition of mitosis', *J. Cell Biol.* **1965**, *25*, 145–160.
[43] G. Indrayanto, G. S. Putra, F. Suhud, 'Validation of in-vitro bioassay methods: Application in herbal drug research', *Profiles Drug Subst. Excip. Relat. Methodol.* **2021**, *46*, 273–307.
[44] N. Weerapreeyakul, A. Nonpunya, S. Barusrux, T. Thitimetharoch, 'Evaluation of the anticancer potential of six herbs against a hepatoma cell lines', *Chin. Med.* **2012**, *7*, 15.
[45] Y. Lu, J. Chen, M. Xiao, W. Li, D. D. Miller, ' An overview of tubulin inhibitors that interact with the colchicine binding site', *Pharm. Res.* **2012**, *29*, 2943–2971.
[46] I. H. Eissa, M. K. Ibrahim, A. M. Metwaly, A. Belal, A. B. Mehany, A. A. Abdelhady, M. A. Elhendawy, M. M. Radwan, M. A. ElSohly, H. Mahdy, 'Design, molecular docking, in vitro, and in vivo studies of new quinazolin-4 (3H)-ones as VEGFR-2 inhibitors with potential activity against hepatocellular carcinoma', *Bioorg. Chem.* **2021**, *107*, 104532.
[47] I. H. Eissa, H. Mohammad, O. A. Qassem, W. Younis, T. M. Abdelghany, A. Elshafeey, M. M. A. R. Moustafa, M. N. Seleem, A. Mayhoub, 'Diphenylurea derivatives for combating methicillin-and vancomycin-resistant *Staphylococcus aureus*', *Eur. J. Med. Chem.* **2017**, *130*, 73–85.
[48] I. H. El Azab, E. M. Saied, A. A. Osman, A. E. Mehana, H. A. Saad, N. A. Elkanzi, 'Novel *N*-bridged pyrazole-1-carbothioamides with potential antiproliferative activity: design, synthesis, *In vitro* and *in silico* studies', *Future Med. Chem.* **2021**, *13*, 1743–1766.
[49] M. G. Salem, D. M. A. El-Maaty, Y. I. M. El-Deen, B. H. Elesawy, A. E. Askary, A. Saleh, E. M. Saied, M. E. Behery, 'Novel 1,3-thiazole analogs with potent activity against breast cancer: A design, synthesis, in vitro, and in silico study', *Molecules* **2022**, *27*, 4898.
[50] T. Mosmann, 'Rapid colorimetric assay for cellular growth and survival: Application to proliferation and cytotoxicity assays', *J. Immunol. Method.* **1983**, *65*, 55–63.
[51] B. A. Abdel-Wahab, H. F. Abd El-Kareem, A. Alzamami, C. A. Fahmy, B. H. Elesawy, M. M. Mahmoud, A. Ghareeb, A. El Askary, H. H. Abo Nahas, N. G. M. Attallah, N. Altwaijry, E. M. Saied, 'Novel exopolysaccharide from marine *Bacillus subtilis* with broad potential biological activities: Insights into antioxidant, anti-Inflammatory, cytotoxicity, and anti-Alzheimer activity', *Metabolites* **2022**, *12*, 715.

Received December 17, 2022
Accepted February 16, 2023